Meas. Sci. Technol. **18** (2007) 3339–3343 doi:10.1088/0957-0233/18/11/012

Analysis of frequency mixing error on heterodyne interferometric ellipsometry

Yuan-long Deng[1,2], Xue-jin Li[1], Yu-bin Wu[1], Ju-guang Hu[1] and Jian-quan Yao[2]

[1] College of Mechatronics and Control Engineering, ShenZhen University, ShenZhen 518060, People's Republic of China
[2] Institute of Laser and Opto-Electronics Engineering, College of Precision Instrument, Tianjin University, Tianjin 300072, People's Republic of China

E-mail: dengyL@szu.edu.cn

Received 28 June 2007, in final form 8 July 2007
Published 20 September 2007
Online at stacks.iop.org/MST/18/3339

Abstract
A heterodyne interferometric ellipsometer, with no moving parts and a transverse Zeeman laser, is demonstrated. The modified Mach–Zehnder interferometer characterized as a separate frequency and common-path configuration is designed and theoretically analyzed. The experimental data show a fluctuation mainly resulting from the frequency mixing error which is caused by the imperfection of polarizing beam splitters (PBS), the elliptical polarization and non-orthogonality of light beams. The producing mechanism of the frequency mixing error and its influence on measurement are analyzed with the Jones matrix method; the calculation indicates that it results in an error up to several nanometres in the thickness measurement of thin films. The non-orthogonality has no contribution to the phase difference error when it is relatively small; the elliptical polarization and the imperfection of PBS have a major effect on the error.

Keywords: ellipsometry, heterodyne interferometer, films measurement, frequency mixing error

(Some figures in this article are in colour only in the electronic version)

1. Introduction

The wide range of applications of thin films with a thickness of nanometres in advanced technologies is becoming increasingly popular as new generations of microelectronics, optical and magnetic devices and materials science and technology are developed. The dynamics of the growth of thin and ultra-thin films and their optical constants are of crucial importance to their performance [1]. Ellipsometers today are making progress in automation in different ways, and are widely used to measure the optical properties of thin films. However, they are still not suitable for the study of a very fast surface process with millisecond or even microsecond resolution, and some kinds of errors are inherent due to the mechanical rotation of optical components [2].

Heterodyne interferometers using a two-frequency laser have been developed for a variety of applications which offer sub-nanometre accuracy, almost unlimited resolution and high anti-interference performance. To overcome the limitations of conventional ellipsometers, many researchers have been intrigued to combine heterodyne interferometry with ellipsometry. In principle, linearly polarized light in the measurement arm of an interferometer is twice reflected from a film, and then recombines at a beam splitter with light from the reference arm. The composite light is spatially separated into p- and s-polarized components before being converted to electrical signals. Hazebroke *et al* produced two heterodyne signals by moving a corner-cube reflector in the reference arm at constant speed [3, 4], and the ellipsometric parameters were obtained from the amplitudes and phase difference. However, the moving reflector driven by an electromechanical device led to some problems [5]. A possible solution to these problems proposed by Wind *et al* was to use a Zeeman laser to generate a beat frequency at 1 MHz [5]. Consequently the ellipsometric parameters showed a fluctuation up to several degrees which arose from frequency

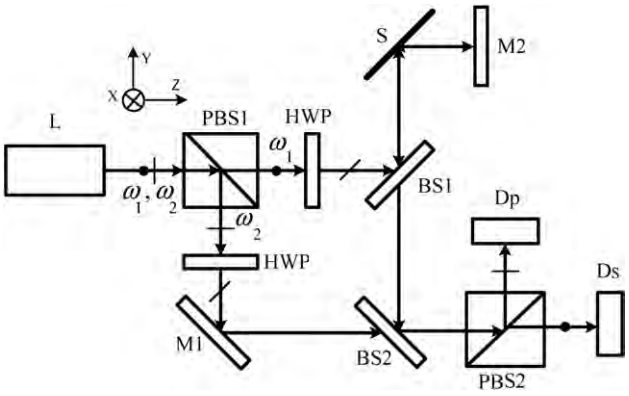

Figure 1. Schematic of the optical configuration. L: Zeeman laser; PBS: polarized beam splitters; HWP: half-wave plate; M: mirrors; BS: beam splitters; S: film sample; D: detector.

mixing error [6, 7]. Two coupled lasers controlled by an external unit were employed to avoid the error [7], as well as a new design of the interferometric ellipsometer using a wavelength-modulated laser diode source [8]. But no further research on the frequency mixing error of interferometric ellipsometers has been reported.

Even though heterodyne interferometers offer resolution up to sub-nanometres, their accuracy is limited by the nonlinear frequency mixing error [9]. The mechanism by which it is created is important for compensating and eliminating the error. Many reports have discussed the error [10–12]. However, they all concentrated on the systems of dynamic displacement measurement using Michelson's setup, and several items of error were only discussed separately. In this paper, a new configuration of reflection ellipsometry was introduced. In terms of the extinction ratios of PBS, elliptical polarization and the non-orthogonality of the light beam, the frequency mixing error in heterodyne interferometric ellipsometers was calculated to explain the fluctuation existing in the experimental results.

Although ellipsometry has been applied to absorbing and anisotropic thin films [2], for simplicity this paper will only focus on non-absorbing and isotropic thin films.

2. Theory and experimental setup

Figure 1 shows a modified Mach–Zehnder interferometer. The transverse Zeeman laser emits two orthogonally linearly polarized beams with a slight angular frequency difference, $\Delta\omega = \omega_2 - \omega_1$. A polarizing beam splitter (PBS1) splits the light into two beams, one for reference and the other for measurement. The transmitted beam at the PBS1 passes through a half-wave plate (HWP), which is set with its fast axis at $\pi/8$ with respect to the X-axis. The polarization of measurement light rotates 45°, so the p- and s-components of the measurement beam with approximately equal intensity are directed towards a film sample via a neutral splitter (BS1) and redirected by a retro-mirror. For the same reason, the HWP in the reference arm is also set with its fast axis at $3\pi/8$ with respect to the X-axis. The p- and s-components of the measurement beam recombine at BS2 with the related components of the reference beam, respectively. After the second polarizing splitter (PBS2) followed by two detectors, the p- and s-components are separated and two sinusoidal signals with a beat frequency $\Delta\omega$ are generated.

The light emitted from the Zeeman laser could be represented as

$$E = \begin{pmatrix}1\\0\end{pmatrix}\exp\left[\mathrm{i}\left(\omega_2 \cdot t + \alpha_2\right)\right] + \begin{pmatrix}0\\1\end{pmatrix}\exp[\mathrm{i}(\omega_1 \cdot t + \alpha_1)] \quad (1)$$

where α_1 and α_2 are the initial phases. By using the Jones matrix method, the response of the optical system can be easily described. The electric field components of the beams incident on the photodetectors D_p and D_s are, respectively,

$$\begin{aligned} E_\mathrm{p} &= P_\mathrm{R} \cdot [B_\mathrm{T} \cdot M \cdot H(3\pi/8) \cdot P_\mathrm{R} \\ &\quad + B_\mathrm{R} \cdot B_\mathrm{T} \cdot S \cdot M \cdot S \cdot B_\mathrm{R} \cdot H(\pi/8) \cdot P_\mathrm{T}] \cdot E \\ E_\mathrm{s} &= P_\mathrm{T} \cdot [B_\mathrm{T} \cdot M \cdot H(3\pi/8) \cdot P_\mathrm{R} \\ &\quad + B_\mathrm{R} \cdot B_\mathrm{T} \cdot S \cdot M \cdot S \cdot B_\mathrm{R} \cdot H(\pi/8) \cdot P_\mathrm{T}] \cdot E \end{aligned} \quad (2)$$

where the subscripts *R* and *T* mean reflection and transmission, *P*, *H*, *B*, *M* and *S* represent the Jones matrixes of the polarizing beam splitters, half-wave plates, beam splitters, mirrors and film sample, respectively,

$$\begin{aligned} P_\mathrm{R} &= \begin{pmatrix}0 & 0\\0 & 1\end{pmatrix} \qquad P_\mathrm{T} = \begin{pmatrix}1 & 0\\0 & 0\end{pmatrix} \\ B_\mathrm{R} &= B_\mathrm{T} = \frac{1}{2}\begin{pmatrix}1 & 0\\0 & 1\end{pmatrix} \qquad S = \begin{pmatrix}r_\mathrm{S} & 0\\0 & r_\mathrm{P}\end{pmatrix} \\ M &= \begin{pmatrix}1 & 0\\0 & -1\end{pmatrix} \qquad H(\pi/8) = \frac{\mathrm{i}}{\sqrt{2}}\begin{pmatrix}-1 & 1\\1 & 1\end{pmatrix} \\ H(3\pi/8) &= \frac{\mathrm{i}}{\sqrt{2}}\begin{pmatrix}1 & 1\\1 & -1\end{pmatrix} \end{aligned} \quad (3)$$

with

$$r_\mathrm{S} = |r_\mathrm{S}| \cdot \exp(\mathrm{i}\phi_\mathrm{S}) \qquad r_\mathrm{P} = |r_\mathrm{P}| \cdot \exp(\mathrm{i}\phi_\mathrm{P}). \quad (4)$$

Equation (4) demonstrates the reflection coefficients of the sample for the p- and s-components, respectively.

Substitution of equations (1), (3) and (4) into equation (2) gives

$$\begin{aligned} E_\mathrm{S} &\propto -\tfrac{1}{4}r_\mathrm{S}^2 \cdot \exp\left[\mathrm{i}\left(\omega_1 t + \alpha_1\right)\right] + \exp\left[\mathrm{i}\left(\omega_2 t + \alpha_2\right)\right] \\ E_\mathrm{P} &\propto -\tfrac{1}{4}r_\mathrm{P}^2 \cdot \exp\left[\mathrm{i}\left(\omega_1 t + \alpha_1\right)\right] + \exp\left[\mathrm{i}\left(\omega_2 t + \alpha_2\right)\right]. \end{aligned} \quad (5)$$

Thus the oscillating terms of intensity signals are obtained:

$$\begin{aligned} I_\mathrm{S} &\propto \tfrac{1}{4}|r_\mathrm{S}|^2 \cdot \cos(\Delta\omega \cdot t - 2\phi_\mathrm{S} + \Delta\alpha) \\ I_\mathrm{P} &\propto \tfrac{1}{4}|r_\mathrm{P}|^2 \cdot \cos(\Delta\omega \cdot t - 2\phi_\mathrm{P} + \Delta\alpha). \end{aligned} \quad (6)$$

The amplitude ratio between I_S and I_P yields $\tan(\psi)$, and the phase difference of the ac signals is equal to 2Δ, i.e,

$$\Delta = \phi_\mathrm{P} - \phi_\mathrm{S} \qquad \tan(\psi) = |\rho| = |r_\mathrm{P}|/|r_\mathrm{S}|. \quad (7)$$

Theoretically speaking, the setup has the advantage of being immune to environmental fluctuation because of the complete common-path configuration.

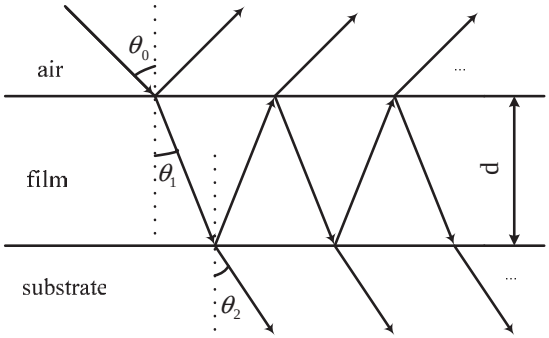

Figure 2. Schematic of the air–film–substrate system ($\lambda = 632.8$ nm, $n_0 = 1.00$, $n_2 = 1.515$, $n_1 = 2.0$, $d = 120.1$ nm, $\theta_0 = 45^\circ$).

Table 1. Experimental data for the single layer ITO.

No.	$\lvert\rho\rvert$	Δ (deg)	n_1	d (nm)
1	0.555	158.7	2.00	120.1
2	0.549	158.2	2.01	121.2
3	0.563	160.1	1.98	118.7
4	0.524	154.9	2.05	124.1
5	0.543	157.6	2.00	122.0
6	0.519	153.5	2.10	123.5
7	0.564	158.7	2.03	118.2
8	0.552	158.7	1.99	120.7
9	0.520	154.0	2.08	123.9
10	0.561	159.8	1.98	119.2

3. Experimental results

The film sample is ITO (indium tin oxide) on a glass substrate, as figure 2 shows.

A scanning probe microscope (CSPM-4000 produced by Benyuan Co, Ltd, vertical resolution: 0.1 nm) with a silicon cantilever was employed to calibrate the film thickness. The measurement results of heterodyne interferometric ellipsometry are demonstrated in table 1.

Obviously, the fluctuation existing in the ellipsometric parameters results in an error up to 5 nm in film thickness measurement. The errors mainly introduced by frequency-mixing are discussed in detail below.

4. Analysis of frequency mixing error

The derivations of section 2 are under ideal conditions, implying that only one frequency occurs in each arm. In practice, various kinds of factors, such as the elliptical polarization and non-orthogonality of light beams, the imperfection and misalignment of the polarized components, together cause frequency mixing in both arms [9], resulting in a nonlinear error in heterodyne interferometers which require nanometre precision.

The ideal output of the transverse Zeeman laser, as figure 3(*a*) shows, could be described as equation (1). Because of elliptical polarization and non-orthogonality, the non-ideal light emitted from the transverse Zeeman laser could be demonstrated as figure 3(*b*). Similar to equation (1), it will be written as

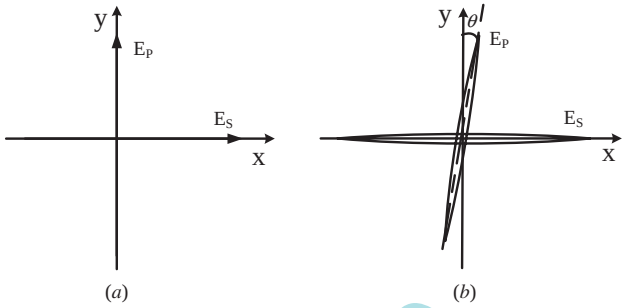

Figure 3. (*a*) Ideal output of the transverse Zeeman laser; (*b*) schematic of elliptical polarization.

$$E = \begin{pmatrix} E_x \\ E_y \end{pmatrix} = \begin{pmatrix} 1 \\ \eta_1 e^{-i\frac{\pi}{2}} \end{pmatrix} \exp[i(\omega_2 t + \alpha_2)] + \begin{pmatrix} \sin\theta - i\eta_2 \cos\theta \\ \cos\theta + i\eta_2 \sin\theta \end{pmatrix} \exp[i(\omega_1 t + \alpha_1)]. \quad (8)$$

The η_1 and η_2 represent the ellipticity of the two modes respectively, and the θ represents the non-orthogonality. In many good metrology grade laser sources, a non-orthogonality of up to 3° has been reported and one finds that the worst case value for η is around 0.05 [11].

Because of imperfection and misalignment, the Jones matrixes of the PBS1 and PBS2 are also modified as

$$P_T^1 = \begin{pmatrix} 1 & 0 \\ 0 & \gamma \end{pmatrix}, \quad P_R^1 = \begin{pmatrix} \gamma & 0 \\ 0 & 1 \end{pmatrix}$$
$$P_T^2 = \begin{pmatrix} 1 & 0 \\ 0 & \kappa \end{pmatrix}, \quad P_R^2 = \begin{pmatrix} \kappa & 0 \\ 0 & 1 \end{pmatrix} \quad (9)$$

where γ and κ represent the extinction ratios of PBS1 and PBS2, respectively.

Substitution of equations (8) and (9) into equation (2) gives the field vector $\boldsymbol{E}_P$ on the photodetector D_p, as equation (10) demonstrates:

$$E_P = \begin{pmatrix} E_P^x \\ E_P^y \end{pmatrix} \propto \begin{pmatrix} \kappa\left(\gamma - \frac{1}{4}r_S^2\right) - i\eta_1\kappa\left(1 + \frac{1}{4}\gamma \cdot r_S^2\right) \\ -\gamma - \frac{1}{4}r_P^2 - i\eta_1\left(1 - \frac{1}{4}\gamma \cdot r_P^2\right) \end{pmatrix} \times \exp[i(\omega_2 t + \alpha_2)] + \begin{pmatrix} (\sin\theta - i\eta_2\cos\theta) \cdot \kappa \cdot \left(\gamma - \frac{1}{4}r_S^2\right) \\ (\sin\theta - i\eta_2\cos\theta) \cdot \left(-\gamma - \frac{1}{4}r_P^2\right) \end{pmatrix} + (\cos\theta + i\eta_2\sin\theta) \cdot \kappa \cdot \left(1 + \frac{1}{4}\gamma \cdot r_S^2\right) + (\cos\theta + i\eta_2\sin\theta) \cdot \left(1 - \frac{1}{4}\gamma \cdot r_P^2\right) \times \exp[i(\omega_1 t + \alpha_1)]. \quad (10)$$

Because η_1, η_2, γ, θ and κ are very small, neglecting the second and higher order terms of η_1, η_2, γ, θ and κ in the field vector expression gives equation (11):

$$E_P = \begin{pmatrix} E_P^x \\ E_P^y \end{pmatrix} \propto \begin{pmatrix} -\kappa \cdot \frac{1}{4}r_S^2 \\ -\gamma - \frac{1}{4}r_P^2 - i\eta_1 \end{pmatrix} \exp[i(\omega_2 t + \alpha_2)] + \begin{pmatrix} \kappa \cdot \cos\theta \\ \cos\theta - \frac{1}{4}r_P^2 \cdot (\sin\theta + \gamma \cdot \cos\theta) + i\eta_2 \cdot \cos\theta \cdot \frac{1}{4}r_P^2 \end{pmatrix} \times \exp[i(\omega_1 t + \alpha_1)]. \quad (11)$$

Then the normalized intensity signal on photodetector D_p may be written as follows:

$$I_P = I_P^x + I_P^y = \tfrac{1}{4}\kappa^2 \cdot |r_S|^2 \cos\theta \cdot \cos(\Delta\omega t + \Delta\alpha - 2\phi_S) + A_1 A_2 \cdot \cos(\Delta\omega t + \Delta\alpha + \phi_1 - \phi_2) \quad (12)$$

where A_i and ϕ_i are given by

$$A_1 \cdot e^{i\phi_1} = -\gamma - \tfrac{1}{4}r_P^2 - i\eta_1$$
$$A_2 \cdot e^{i\phi_2} = \cos\theta - \tfrac{1}{4}r_P^2 \cdot (\sin\theta + \gamma \cdot \cos\theta) + i\eta_2 \cdot \cos\theta \cdot \tfrac{1}{4}r_P^2. \quad (13)$$

Similarly, the intensity signal on D_s can be derived:

$$I_S = I_S^x + I_S^y = A_3 \cdot A_4 \cos(\Delta\omega t + \Delta\alpha + \phi_3 - \phi_4) + \tfrac{1}{4}\kappa^2 \cdot |r_P^2| \cos\theta \cdot \cos(\Delta\omega t + \Delta\alpha - 2\phi_P) \quad (14)$$

and

$$A_3 \cdot e^{i\phi_3} = \gamma - \tfrac{1}{4}r_S^2 - i\eta_1$$
$$A_4 \cdot e^{i\phi_4} = \cos\theta - \tfrac{1}{4}r_S^2 \cdot (\sin\theta - \gamma\cos\theta) + i\eta_2 \cdot \cos\theta \cdot \tfrac{1}{4}r_S^2. \quad (15)$$

From equations (12)–(15), it is clear that I_P^x and I_S^y are much less than I_P^y and I_S^x, respectively. After omitting I_P^x and I_S^y, the measuring error of the ellipsometric parameters may be derived from equations (7), (12) and (14):

$$\delta|\rho| = \sqrt{\frac{A_1 A_2}{A_3 A_4}} - \frac{|r_P|}{|r_S|}$$
$$\delta\Delta = \frac{[(\phi_1 - \phi_2) - (\phi_3 - \phi_4)]}{2} - \Delta. \quad (16)$$

Obviously, the errors vary with r_P and r_S. According to equations (12) and (14), the intensity signals are just related to κ^2, so the PBS2 only produces higher order error.

5. Discussion

To assume $\eta_1 = \eta_2 = 0$ and $\theta = 0°$, and substitute the specification of the sample into equation (16), the ellipsometric parameter errors produced by the imperfection of PBS1 are demonstrated in figure 4. The ellipsometric parameter errors are approximately linear to the imperfection of PBS1 while γ has a magnitude of 10^{-4}. γ of about 3×10^{-4} will produce

$$\delta\Delta \approx 0.4° \qquad \delta|\rho|/|\rho| \approx 1\% \quad (17)$$

Substitution of equation (17) into the fundamental ellipsometry equations [2] gives an error of thickness measurement of about 1 nm.

To assume $\gamma = 0$ and $\eta_1 = \eta_2 = \eta$, figures 5 and 6 describe the rule between the errors and ellipticity η and non-orthogonality θ. Taking into account the items γ, η and θ synchronously, the errors of the ellipsometric parameters are calculated in table 2. Figure 5 and table 2 suggest that the ellipticity η approximately alone is responsible for the nonlinear phase difference error when the non-orthogonality θ is relatively small, but the non-orthogonality does affect the error of amplitude ratio, according to figure 6 and table 2. In sum the ellipticity η has more important contributions than non-orthogonality to the errors of the ellipsometric parameters.

The ellipsometric parameter errors are also approximately linear to the η while it is very small. In figures 5 and 6, η, θ of about 2×10^{-3} and 6°, respectively, will produce

$$\delta\Delta \approx 1.5° \qquad \delta|\rho|/|\rho| \approx 4\% \quad (18)$$

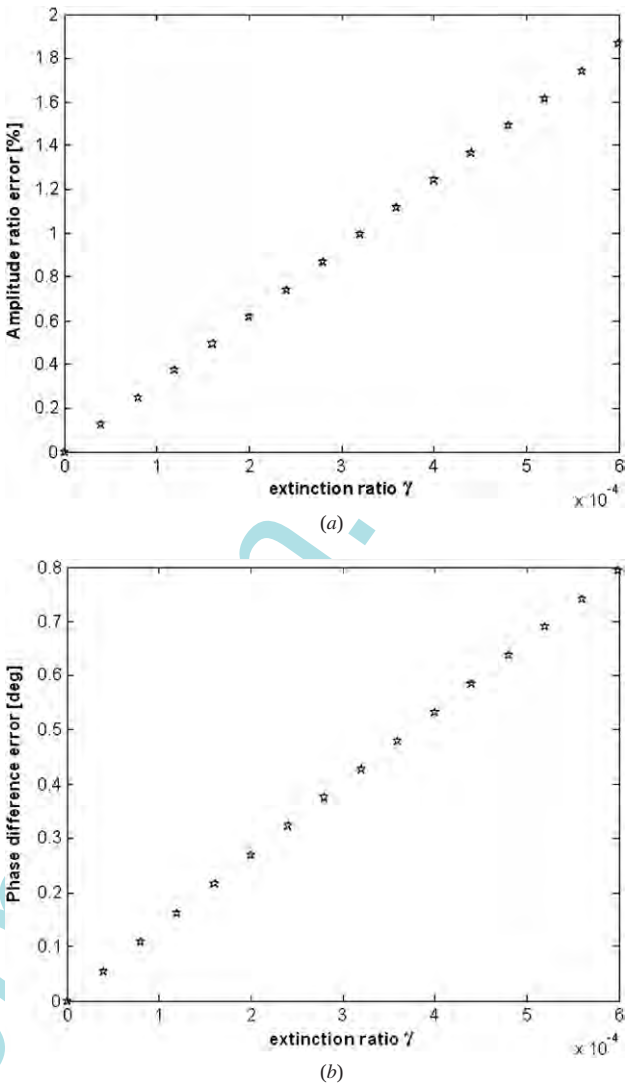

Figure 4. (*a*) Amplitude ratio error versus imperfection of PBS1; (*b*) phase difference error versus imperfection of PBS1.

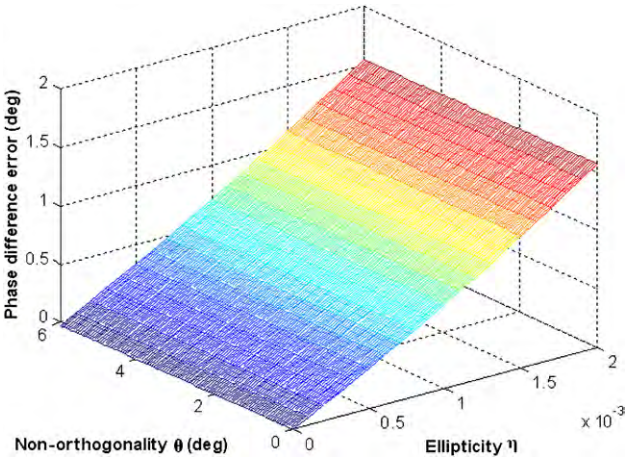

Figure 5. Phase difference error versus ellipticity η and non-orthogonality θ.

Similarly, now the error of the thickness measurement is about 4 nm, according to the fundamental ellipsometry equations.

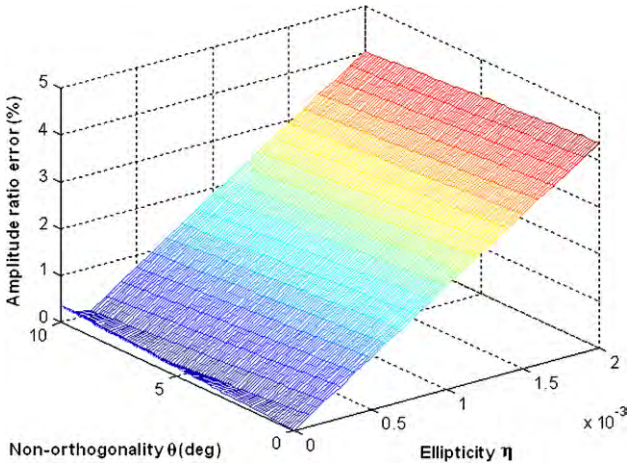

Figure 6. Amplitude ratio error versus ellipticity η and non-orthogonality θ.

Table 2. Effect of the extinction ratio, ellipticity and non-orthogonality on the ellipsometric parameter error.

Extinction ratio γ	Ellipticity η	Non-orthogonality θ (deg)	$\delta\Delta$ (deg)	$\delta\|\rho\|/\|\rho\|$ (%)
6×10^{-4}	0.002	3	2.3	−2.2
3×10^{-4}	0.001	1	1.1	−1.2
10^{-4}	0.0005	1	0.5	−0.75
0.0005	0.0005	1	1.0	0.52
0.0005	0.0005	3	1.0	0.59

Comparing the figures 4–6 with table 2, one can find that the total errors produced by γ, η and θ synchronously are not equal to the sum of the individuals. Namely, their influence on measurement accuracy is cross-correlated, and to discuss the influence separately does not make sense.

Because the PBS2 only produces higher order error, comparatively speaking it is less important.

6. Conclusion

A heterodyne interferometric ellipsometer using a transverse Zeeman laser was presented. Without any rotational mechanical parts, the measurement system is expected to operate at higher speed and stability. The complete common-path configuration is helpful to improve the anti-interference performance; so the system is more applicable to *in situ* and real time measurement than conventional ellipsometers. The experimental results show a fluctuation of about 5 nm in film thickness measurement.

A full analysis based on the Jones matrix method was carried out on the nonlinear frequency mixing error. The imperfection and misalignment of PBS, elliptical polarization and non-orthogonality of the light beam together give rise to an error of up to several nanometres in film thickness measurement.

In fact γ, η_i and θ are not constants, they vary a little with environmental parameters [13]. Therefore, the frequency mixing error always appears to be a quasi-periodical fluctuation. Although the drift of the errors was not studied in this paper, the results are expected to be useful when artificial intelligence, such as neural network and genetic algorithms, is applied to compensating and eliminating the error [14].

Acknowledgments

The authors would like to thank Professor Ji-bin Li and his graduate Fei Luo for their help on using AFM, and Professor Xiu-quan Sun's contributions to this work. The funding by the ShenZhen Science and Technology Program is gratefully acknowledged.

References

[1] Auciello O and Krauss A R 2001 *In Situ Real-Time Characterization of Thin Films* (New York: Wiley)
[2] Azzam R M A and Bashara N M 1996 *Ellipsometry and Polarized Light* (Amsterdam: North-Holland)
[3] Hazebroek H F and Visser W M 1983 Automated laser interferometric ellipsometry and precision reflectometry *J. Phys. E: Sci. Instrum.* **16** 654–61
[4] Hazebroek H F and Holscher A A 1973 Interferometric ellipsometry *J. Phys. E: Sci. Instrum.* **6** 822–6
[5] Wind M M and Hemmes K 1994 New ultra-fast Interferometric ellipsometry system based on Zeeman two-frequency laser *Meas. Sci. Technol.* **5** 37–46
[6] Deng Y *et al* 2005 Study of heterodyne ellipsometry for nanometer film measurement *Opt. Tech.* **31** 391–3 (in Chinese)
[7] Hemmes K *et al* 1998 Evaluation of interferometric ellipsometer systems with a time resolution of one microsecond and faster *Thin Solid Films* **40–46** 313–4
[8] Watkins L R and Hoogerland M D 2004 Interferometric ellipsometer with wavelength-modulated laser diode source *Appl. Opt.* **43** 4362–6
[9] Wu C-M and Su C-S 1996 Nonlinearity in measurements of length by optical interferometry *Meas. Sci. Technol.* **7** 62–8
[10] Hou W and Wilkening G 1992 Investigation and compensation of the nonlinearity of heterodyne interferometers *Precis. Eng.* **14** 91–8
[11] De Freitas J M 1997 Analysis of laser source birefringence and dichroism on nonlinearity in heterodyne interferometry *Meas. Sci. Technol.* **8** 1356–9
[12] Eom T B *et al* 2002 A simple method for the compensation of the nonlinearity in the heterodyne interferometer *Meas. Sci. Technol.* **13** 222–5
[13] Dai G L, Yin C Y and Xie G P 1998 Study on drift of nonlinearity in nanometer precision heterodyne interferometers *Acta Opt. Sin.* **18** 1697–702 (in Chinese)
[14] Li Z, Herrmann K and Pohlenz F 2003 A neural network approach to correcting nonlinearity in optical interferometers *Meas. Sci. Technol.* **14** 376–81